FE simulation of a cord-rubber composite tube subjected to bending due to operational loads on a railroad reverse curve with extremely low curve radius at sub-zero temperature

Gyula Szabó, Károly Váradi
Department of Machine and Product Design
Budapest University of Technology and Economics
1-3 Műegyetem Quai, Budapest 1111, Hungary
E-mail:szabo.gyula@gt3.bme.hu

KEYWORDS
filament-wound composite tube, cord-rubber tube, railway brake tube, bending, FE model, cold environment, reverse curve

ABSTRACT

The aim of this study is to examine railway brake tubes subjected to bending due to operation on a railroad reverse curve with extremely low curve radius in case of critical load cases at -40°C. Firstly, kinematic simulation has been performed in order to determine the input prescribed displacements of the FE simulation. Then, FE model is presented for the critical positions, without and with internal pressure. Stress and strain states have been analysed. Finally, a standard deflection test has been carried out along with the FE model of the deflection test based on the material model of the FE model of bending for experimental validation.
Tsai-Hill failure indices are lower than 1 and equivalent stresses in rubber liners are lower than tensile strength of rubber for all load cases, so material failure is not imminent regarding such extreme operating conditions. With internal pressure applied, maximum failure indices tend to be lower. The deflection test results are in good agreement with the corresponding FE model deflection results, validating FE model of operation (reverse curve, -40 °C).

INTRODUCTION

Composite tubes are applied in a great number of industrial fields; in transportation, oil industry and aeronautics due to their high specific strength and high specific stiffness [1]. The most extensively utilized manufacturing technology of cord-rubber tubes is filament-winding because of high fiber precision, and being well-suited to automation [2]. The most common operational loads are uniaxial tension, internal pressure, biaxial tension and bending [3]. The most frequently applied conventional winding angle is ±55°, which is the optimal one related to biaxial tension. [4] Filament-wound cord-rubber composite tubes are extensively used as railway brake pipes because of their high specific strength, high flexibility and relatively low cost. During railway operation, brake tubes are subjected to high bending loads in railway tracks with extremely low curvature radius. In cold environment, their mechanical behaviour is also stiffer, because of elevated matrix stiffness, resulting in even higher loads and possible material failure. The aim of this study is to examine stress and strain states of railway brake tubes in case of critical load cases at -40°C. Railway brake tubes can be seen in *Figure 1* mounted on railway carriages.

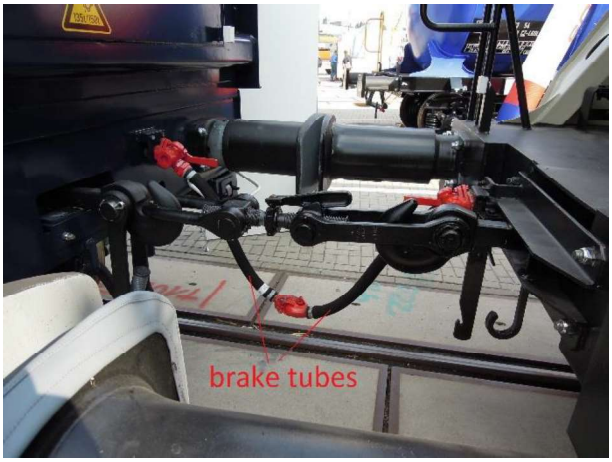

Figure 1. Illustration of railway brake tubes mounted on railway carriages

KINEMATIC SIMULATION

Tubes are actuated by positioning pins throughout the operation. For determination of the location of suspension points of the positioning pins (representing couplings), a kinematic simulation has been performed in PTC Creo 2.0 Mechanism environment as it is used in engineering practice. The kinematic model consists of railway carriages traveling on railway tracks having an arc with a radius of 80 m and two straight sections (*Figure 2*). This curve radius is regarded as extremely low in railway construction practice.

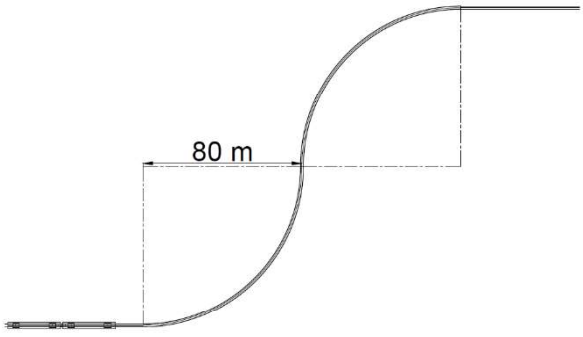

Figure 2. Schematic diagram of the railway track in the kinematic simulation

Communications of the ECMS, Volume 33, Issue 1,
Proceedings, ©ECMS Mauro Iacono, Francesco Palmieri,
Marco Gribaudo, Massimo Ficco (Editors)
ISBN: 978-3-937436-65-4/978-3-937436-66-1(CD) ISSN 2522-2414

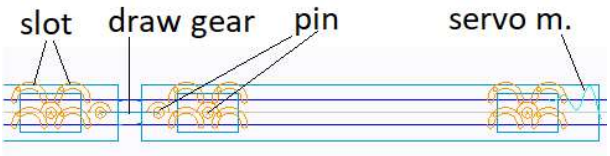

Figure 3. Schematic diagram of the kinematic model with constraints

Figure 3 shows arrangement of the railway cars and bogies on the railway track. Bogies are connected to the railway tracks by *slot* constraints at the two sides of each bogie representing railway wheels. Connection of the bogies to a carriage is *pin*, with a maximum permitted rotation of 10° [5], representing center pivots. The carriages are connected to one another by a *draw gear*, a part able to rotate around fixed points in the carriages. The right bogie of the right railway carriage contains a *servo motor* for actuating the assembly on the railway tracks. Dimensions of the kinematic simulation have been determined based on railway standards [6], [7] and data of Siemens SF 400 bogie [8], *see Figure 4*.

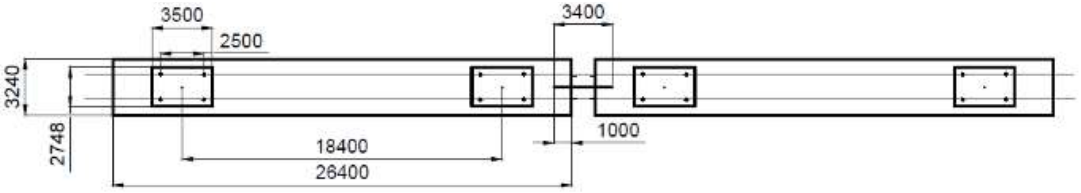

Figure 4. Representation of the kinematic model with dimensions

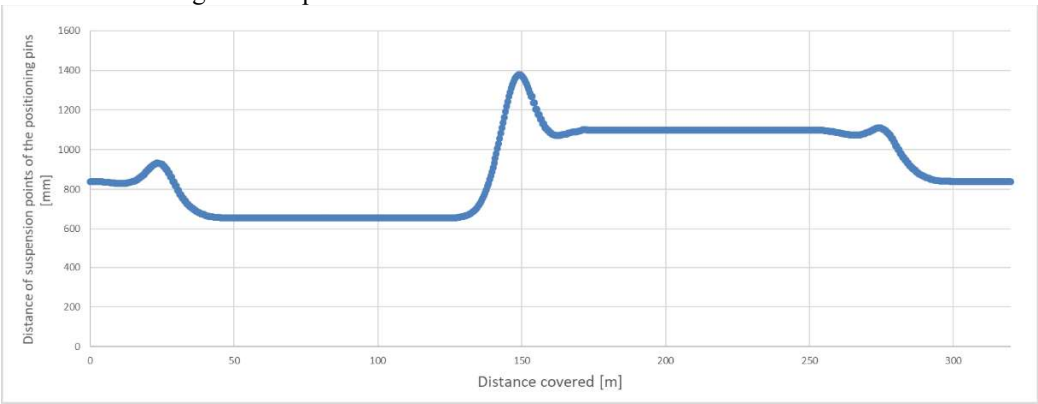

Figure 5. Distance of suspension points of the positioning pins

In the initial point of the kinematic simulation, the distance of the suspension points of the positioning pins on the carriages is 840 mm. In *Figure 5*, this distance can be seen related to the left pair of tubes as a function of distance covered. At first, this distance decreases because that pair of tubes is on the inner side of the railway track. In the second half, the left pair of tubes is on the outer side of the track, therefore, the distance is higher. In the middle of the kinematic simulation, the distance of the suspension points increases extremely, because the front carriage and the back carriage are on curved tracks having opposite curvatures. The worst cases are the minimum and maximum distances of the suspension points throughout the kinematic simulation, so these cases are needed to be examined in terms of loads, stress and strain states. These extremums are: 655 mm and 1379 mm.

Position results of the kinematic simulation can be seen in *Figure 6* (for minimum suspension point distance) and in *Figure 7* (for maximum suspension point distance).

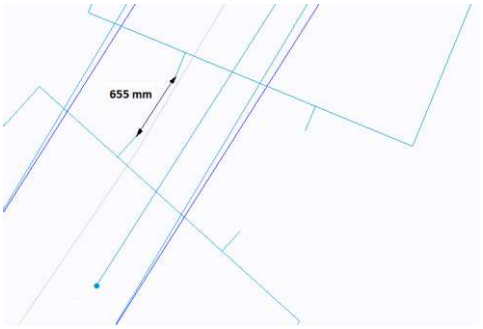

Figure 6. Railway cars at minimum suspension point distance

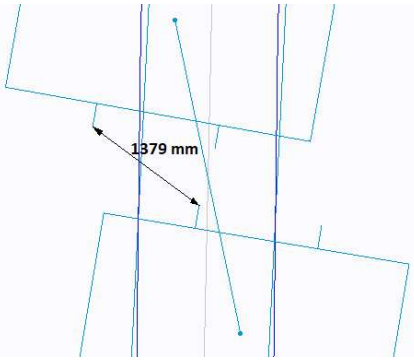

Figure 7. Railway cars at maximum suspension point distance

FE MODEL

Length of both tubes is 620 mm. The tube consists of composite reinforcement layers and rubber liners (*Figure 8*). The inner diameter of the tube is 28 mm, its outer diameter is 44 mm, the thickness of the rubber liners is 2.4 mm. The material coordinate system of the reinforcement layers is cylindrical, the layup is [+55°/-55°/+55°/-55].

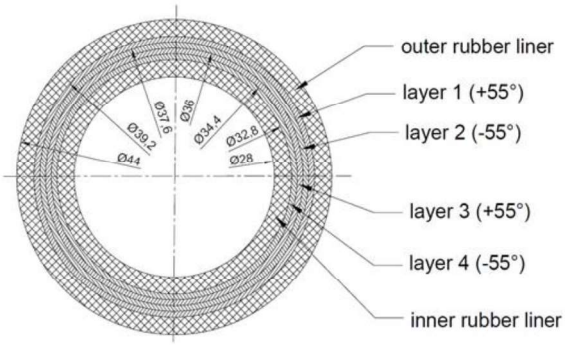

Figure 8. Cross-section of the tube [9]

Material model of reinforcement layers is transversely isotropic, material properties of the composite layers have been calculated based on mixture rules [10] and material properties of the components [11]. Material properties of components of reinforcement layers are as follows: modulus of elasticity of fibre is E_f=2961 MPa, Poisson's ratio of fibre is supposed to be υ_f=0.2, modulus of elasticity of rubber matrix is $E_m=E_r$= 19.1 MPa. E_1=1345 MPa, $E_2=E_3$=57 MPa, $\upsilon_{12}=\upsilon_{13}$=0.3637, υ_{23}=0.496, $G_{12}=G_{23}=G_{13}$=19 MPa. Rubber liners, made of EPDM-EVA compound, regarded as incompressible, have been described by a 2 parameter Mooney-Rivlin model with parameters C_{10}=3,34 MPa, C_{01}=1,077 MPa, D=0 1/MPa. These material properties have been validated previously by uniaxial tensile tests performed on test specimens and tube pieces.[11]
Rubber is vulcanized around yarns, so connection of inner and outer rubber liners to reinforcement layers is bonded.

Figure 9. Prescribed displacements in front view and top view

Actuation of the tubes is realized by prescribed displacements (*Figure 9*) of the suspension points of the positioning pins, which have been determined by the kinematic simulation. The tubes are connected to one another in the middle by a fixed joint of holes of two positioning pins, whose distance is 10 mm in direction Z.

Table1. Prescribed displacements of FE model without internal pressure

	translation X [mm]	translation Z. [mm]	rotationY [°]
min. s. d. left	242.7	33.5	9.3
min. s. d. right	-242.7	-33.5	-9.3
max. s.d. left	278.6	615.86	-3. 7
max.s.d. right	-278.6	-615.86	-3.7

where *min. s. d. left* is the abbreviation of minimum suspension point distance load case-left remote point *max. s. d. left* is the abbreviation of maximum suspension point distance load case-left remote point

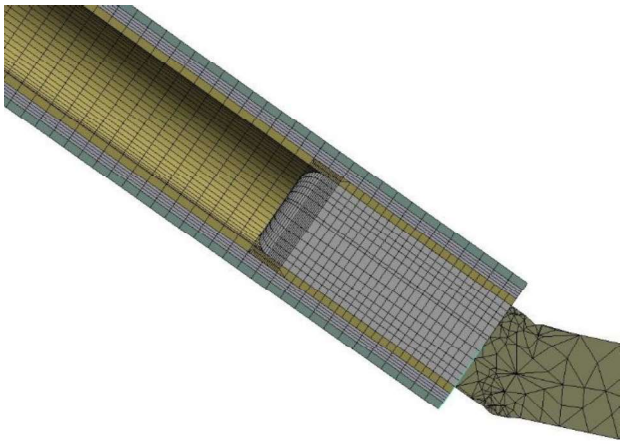

Figure 10. Meshed FE model at the tube-positioning pin contact

The Finite Element model consists of 151548 nodes, 110800 SOLID185 hexahedral elements and 50260 SOLID 187 tetrahedral elements, a detail of the mesh can be seen in *Figure 10*. (The positioning pin consists of two bodies, bonded to one another, due to meshing considerations.)
At t=0 s of the FE simulation, the distance of the suspension points of the positioning pins is 1140 mm, derived from [7]. Prescribed displacements for minimum and maximum suspension point distance load cases are listed in *Table 1* relative to the initial configuration.
We further investigated the load case of additional internal pressure in case of the minimum and maximum suspension point distances (*Figure 11*). By exploiting the symmetry of the model, in these examinations, only a half model has been considered (the left tube and its pins). The pressure load is 5 bar, the displacement of the connecting remote point (in the middle) and the displacement of the suspension point of the positioning pin match those of the displacement results of the simulation without internal pressure. This simulation

consists of two time steps. In the first one, an internal pressure of 5 bar is applied to the inner lateral surface of the tube, while in the second one, the prescribed displacement results are applied.

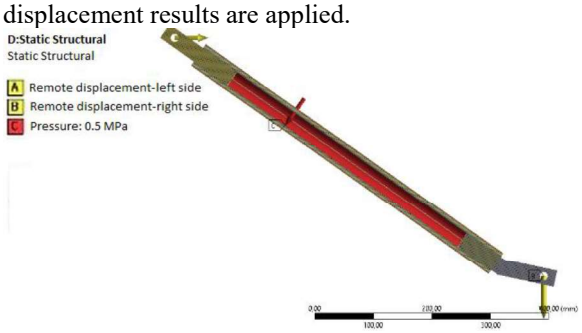

Figure 11. Half FE model with internal pressure

Failure behaviour has been analysed with Tsai-Hill failure criterion. Tsai-Hill criterion is widely utilized for describing failure behaviour of cord-rubber composites [12]. Tsai-Hill criterion [13] is the maximum work criterion, an extension of the von Mises criterion (based on the stored distortional energy) to anisotropic materials with the utilization of strength properties in material directions (listed below). Criterial equation for the Tsai-Hill theory for 3D case is as follows [14] [15]:

$$\frac{{\sigma_1}^2}{X^2}+\frac{{\sigma_2}^2}{Y^2}+\frac{{\sigma_3}^2}{Z^2}-\sigma_1\cdot\sigma_2\cdot\left(\frac{1}{X^2}+\frac{1}{Y^2}-\frac{1}{Z^2}\right)-\sigma_1\cdot\sigma_3\cdot\left(\frac{1}{X^2}-\frac{1}{Y^2}+\frac{1}{Z^2}\right)-\sigma_2\cdot\sigma_3\cdot\left(-\frac{1}{X^2}+\frac{1}{Y^2}+\frac{1}{Z^2}\right)+\frac{{\tau_{23}}^2}{Q^2}+\frac{{\tau_{13}}^2}{R^2}+\frac{{\tau_{12}}^2}{S^2}<1 \quad (1)$$

where
X, *Y* and *Z* are tensile/compressive strength values in material direction 1, 2 and 3 respectively
Q, *R* and *S* are shear strength values in planes 23, 13 and 12 respectively

$X = X_t$ *tensile strength*, if the stress is tensile, $X_1 = X_c$ *compressive strength*, if the stress is compressive

If failure index is less than 1, failure does not occur. The strength properties are the following:
$R_{m,y}$=342.5 MPa (ultimate tensile strength of the yarn, derived from the uniaxial tensile test of the composite tube at room temperature [9]), $R_{m,r}$=11 MPa (ultimate tensile strength of the rubber matrix, derived from the uniaxial tensile test of the composite tube at -40°C [11]). Strength properties in material directions are as follows:
$X_t=X_c$=342.5 MPa , $Y_t= Y_c=Z_t= Z_c$=34.2 MPa (assuming strength is much lower in transverse directions); Q=R=S=5.5 MPa, derived from the strength of the rubber (half of the strength of the rubber)

DEFLECTION TEST AND ITS FE MODEL

Deflection test has been carried out according to [16] along with an FE model of the deflection test in order to validate the FE model of bending of tubes in operational conditions presented beforehand. The test assembly comprises of the tube, gripped in a clamp, and a weight placed inside a stopper at the free end of the tube (*Figure 12*). The test assembly had been placed inside a climate chamber at a temperature of -40°C for 12 hours. At the beginning of the test, the yarn has been cut, applying the load, vertical deflection has been measured and recorded after 10 s. The measured deflection has been 15 mm.

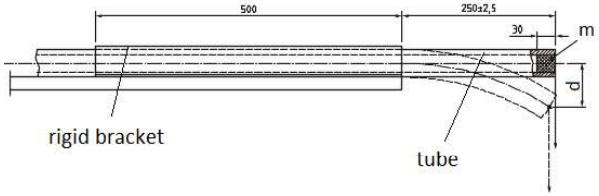

Figure 12. Schematic diagram of test rig for deflection at low temperature [16]

d: deflection of the tube
m: stopper with location for weight (*mass* of 2 kg*)*

A deflection simulation, being a nonlinear static simulation has also been performed based on the dimensions of the test assembly and the FE model of the tube presented beforehand. The deflection simulation consists of the tube, the rigid bracket and the mass. The rigid bracket is fixed and the tube is bonded into the inner lateral surface of it (*Figure 13*). There is a 20 N load applied to the mass at its center of gravity.

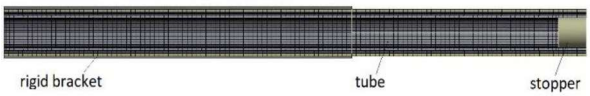

Figure 13. Meshed FE model of deflection

THERMAL STRESSES

A thermomechanical model of one tube has been created in order to inspect thermal stresses attributed to thermal expansion effects (contraction) because the assembly is cooled to -40 °C from room temperature (22°C).

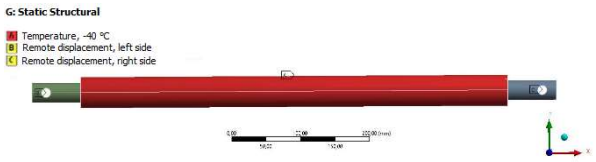

Figure 14. Thermomechanical model of the brake tube

A temperature boundary condition of -40°C has been applied to the outer lateral surface of the brake tube, and the left remote point is fixed, while the right remote point has a free degree of freedom in X direction (Figure 14).

RESULTS

RESULTS WITHOUT INTERNAL PRESSURE

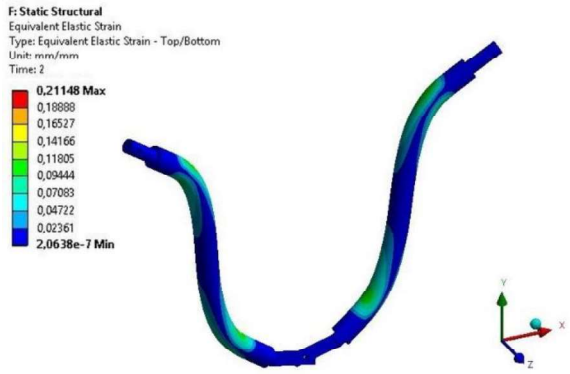

Figure 15. Equivalent strain results for minimum suspension point distance with deformed shape (deformation scale 1:1)

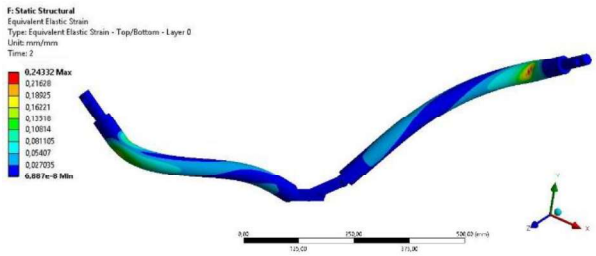

Figure 16. Equivalent strain results for maximum suspension point distance with deformed shape, (deformation scale 1:1)

Equivalent strain results can be seen in *Figure 15* for minimum suspension point distance and those for maximum suspension point distance in *Figure 16* along with deformed shapes.

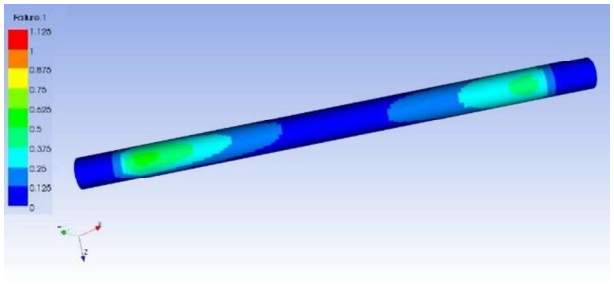

Figure 17. Tsai-Hill failure index distribution in case of minimum suspension point distance

Maximum failure index is 0.54 in case of minimum suspension point distance (*Figure 17*), arising at the bent curve of the tube, being far below the criterial value 1, therefore failure is not imminent in this load case for composite plies.

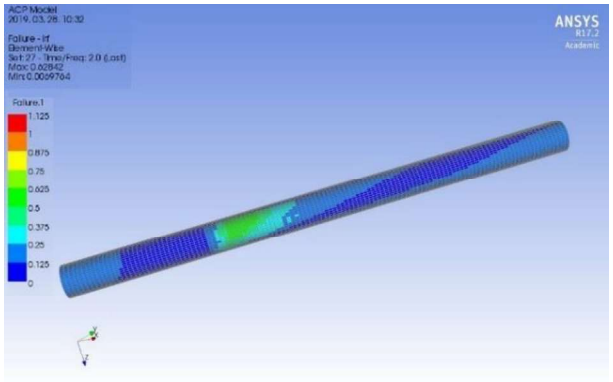

Figure 18. Tsai-Hill failure index distribution in case of maximum suspension point distance

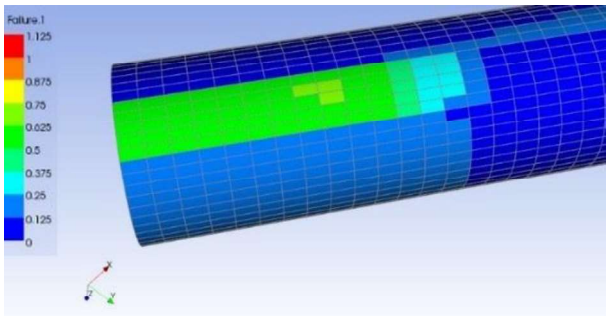

Figure 19. Tsai-Hill failure index distribution in case of maximum suspension point distance, in the vicinity of the maximum value (rear view)

In case of maximum suspension point distance, due to bending and torsional loads, a local maximum failure index of 0.58 can be seen between the positioning pins (*Figure 18*). Overall maximum failure index is 0.628, occuring in the outermost layer near the contact of the positioning pin and the tube (*Figure 19*). This value is below 1, so failure is not probable in this load case either.

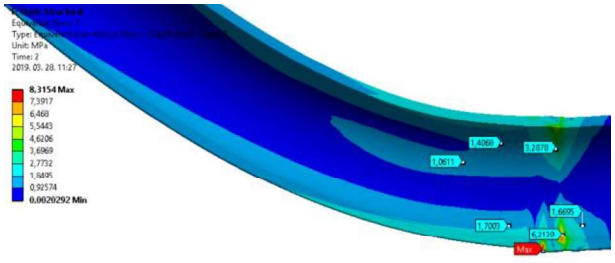

Figure 20. Equivalent stress in the inner rubber liner, minimum suspension point distance, in lateral section

Maximum equivalent stress arises in the inner rubber liner in case of minimum suspension point distance (Figure 20), having a value of 8 MPa constrained to a small area. This value is below the ultimate tensile strength of the rubber at -40°C.

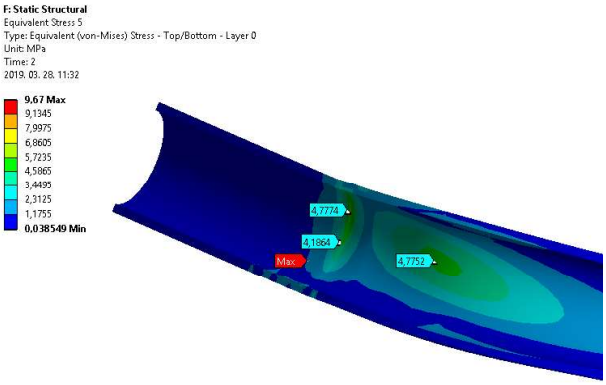

Figure 21. Equivalent stress in the inner rubber liner, minimum suspension point distance, in lateral section

In case of maximum suspension point distance (*Figure 21*) , maximum equivalent stress also occurs in the inner rubber liner. The maximum value is under the critical value in this case.

RESULTS WITH INTERNAL PRESSURE

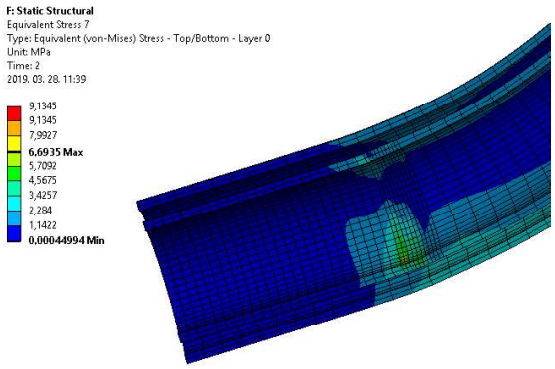

Figure 22. Equivalent stress in rubber liners, minimum suspension point distance with internal pressure applied, in lateral section

In *Figure 22*, equivalent stress distribution can be seen for rubber liners. These stress values are much lower than the tensile strength of the rubber, therefore material failure is not expected.

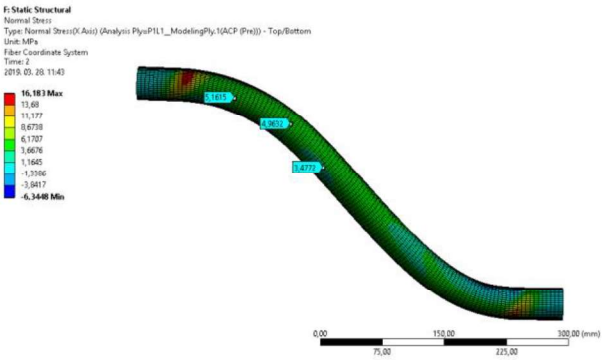

Figure 23. Normal stress in material direction 1 in the outermost layer, minimum suspension point distance with internal pressure

Normal stresses in material direction 1 are considerable (*Figure 23*), having the same magnitude as stresses arising in case of the tube piece subjected to uniaxial tension of 30 mm. [11]

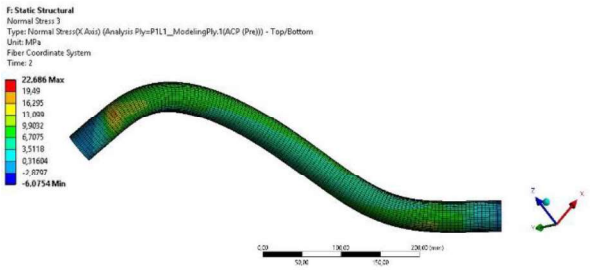

Figure 24. Normal stress in material direction 1 in the outermost layer, maximum suspension point distance with pressure

In case of maximum suspension point distance (*Figure 24*) , stresses reach 16 MPa, which is considerable though far lower than the strength limit.

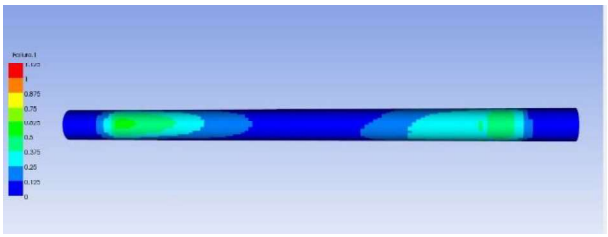

Figure 25. Tsai-Hill failure index distribution in case of minimum suspension point distance, with internal pressure

Tsai-Hill failure index distribution is almost symmetric in case of minimum suspension point distance with internal pressure applied (*Figure 25*), the maximum failure index (0.53) being slightly lower than with no internal pressure (0.54).

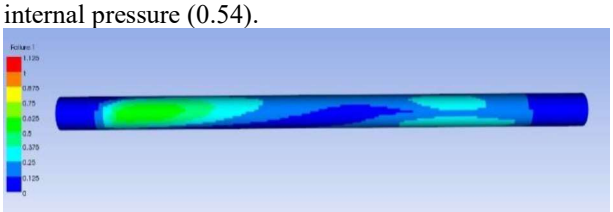

Figure 26. Tsai-Hill failure index distribution in case of maximum suspension point distance, with internal pressure

In case of maximum suspension point distance (*Figure 26*), the resulting failure index distribution is asymmetric as in case of no internal pressure applied because there is a significant torsion due to the prescribed displacements. Maximum failure index is slightly lower than in case of no pressure applied.

RESULTS OF THE DEFLECTION TEST

The maximum vertical deformation of the deflected tube is -16.5 mm (*Figure 27*) which is 10% higher than

experimental results showing fairly good agreement, justifying the appropriateness of FE results of operational conditions.

Figure 27. Vertical deformation of the deflected tube

THERMAL STRESS RESULTS

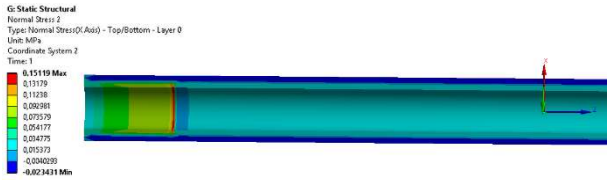

Figure 28. Thermal stresses in radial direction (X)

Thermal stresses in radial direction (X) (Figure 28) are not significant, therefore the effect of thermal contraction can be neglected in the FE models detailed above.

CONCLUSIONS

Prescribed displacement values, dependent on the kinematic simulation, and cold environment (-40°C) represent extreme operational conditions. Material failure indices in reinforcement layers and equivalent stress values in rubber liners show that the arising stress values are below the permissible stress limits, therefore the analysed composite tube is still applicable in these load cases and will probably not undergo material failure. Maximum failure indices tend to be slightly lower in case of internal pressure applied, although the domain in which the maximum value is situated tends to be larger in that case, therefore the effect of internal pressure seems to be beneficial because stress concentration is reduced.

FE model of operational bending on a reverse curve with extremely low curve radius at low temperature has been validated by standard deflection test and its FE counterpart.

Thermal stresses attributed to thermal expansion can be neglected because the stresses in radial direction of the tube are not significant based on the thermomechanical model.

ACKNOWLEDGEMENT

Authors would like to express their gratitude to Attila Piros, Department of Machine and Product Design at the Budapest University of Technology and Economics for his valuable assistance in the creation of the kinematic simulation.

The recent study and publication were realized within the Knorr-Bremse Scholarship Program supported by the Knorr-Bremse Rail Systems Budapest.

REFERENCES

[1] Braiek S, Zitoune R, Ben Khalifa A, et al. 2017; Experimental and numerical study of adhesively bonded ±55° filament wound tubular specimens under uniaxial tensile loading. *Compos Struct* 172: 297–310. DOI: https://doi.org/10.1016/j.compstruct.2017.03.103

[2] Almeida JHS, Ribeiro ML, Tita V, et al. 2017, Damage modeling for carbon fiber/epoxy filament wound composite tubes under radial compression. *Compos Struct*; 160 :204–210. DOI: https://doi.org/10.1016/j.compstruct.2016.10.036

[3] Menshykova M, Guz IA. 2014 Stress analysis of layered thick-walled composite pipes subjected to bending loading *Int J Mech Sci*; 88: 289–299. DOI: https://doi.org/10.1016/j.ijmecsci.2014.05.012

[4] Soden PD, Kitching R, Tse PC. 1989 Experimental failure stresses for ±55° filament wound glass fibre reinforced plastic tubes under biaxial loads *Composites*; 20 (2): 125–135. DOI: https://doi.org/10.1016/0010-4361(89)90640-X

[5] Shi H., Ping-bo Wu P., Ren L. and Guo J. 2015, Calculation and laboratory testing of the rotation resistance of a bogie, *J Rail and Rapid Transit*, , Vol. 229, (2) 210–219, https://doi.org/10.1177/0954409713508110

[6] UIC 541-1 Regulations concerning the design of break components

[7] UIC 520 -Wagons, coaches and vans-Draw gear-Standardisation

[8] First Class Bogies The complete programme for high-quality railway transportation, Siemens catalogue https://www.mobility.siemens.com/mobility/global/sitecollectiondocuments/en/rail-solutions/components-and-systems/bogies-catalog-en.pdf

[9] Szabó, G., Váradi, K. and Felhős, D. 2017 Finite Element Model of a Filament-Wound Composite Tube Subjected to Uniaxial Tension *Modern Mechanical Engineering*; 7 (4): 91–112. DOI:10.4236/mme.2017.74007

[10] Chawla, K. K. *Composite Materials Science and Engineering* (3rd Ed.). New York; London: Springer. 2009

[11] Szabó, G. and Váradi, K. 2018 Uniaxial Tension of a Filament-wound Composite Tube at Low Temperature, Acta Technica Jaurinensis, 11 (2), pp. 84-103. doi: 10.14513/actatechjaur.v11.n2.456

[12] Rao, S., Daniel, I.M. & Gdoutos, E.E. 2004 Mechanical Properties and Failure Behavior of Cord/Rubber Composites *Applied Composite Materials* 11: 353. https://doi.org/10.1023/B:ACMA.0000045312.61921.1f

[13] Reddy, J.N., Soares C.A.M et al. *Mechanics of Composite Materials and Structures*, Springer. 1999

[14] Jones, R.M., *Mechanics of Composite Materials*, Taylor&Francis, 1999

[15] Ansys Documentation, Ansys Composite Preppost User's Guide, Failure Criteria for Reinforced Materials, Tsai-Hill criterion

[16] Railway applications-Pneumatic half couplings. EN 15807:2011 BSI Standard

GYULA SZABÓ is a PhD Student at the Faculty of Mechanical Engineering, Budapest University of Technology and Economics. His research interests include finite element modelling, composites, particularly cord rubber tubes and diaphragms.

KÁROLY VÁRADI is a professor at the Department of Machine and Product Design, Budapest University of Technology and Economics. His research interests include finite element modelling, structural analyses, composites, fracture mechanics and biomechanics.